SIMULATION OF CMP SEISMIC SECTIONS

J.M. CARCIONE, G. BOEHM and A. MARCHETTI

Osservatorio Geofisico Sperimentale, P.O. Box 2011 Opicina, 34016 Trieste, Italy.

(Received March 2, 1994; revised version accepted September 8, 1994)

ABSTRACT

Carcione, J.M., Boehm, G. and Marchetti, A., 1994. Simulation of CMP seismic sections. *Journal of Seismic Exploration*, 3: 381-396.

In the design of data-processing techniques it is often necessary to compute a zero-offset section of a given geological model in order to test the performance of the algorithm. In this work, we compare different approaches to obtaining a zero-offset or CMP seismic section from synthetic data. The correct but expensive way is to compute a set of common-shot seismograms and perform the CMP stacking. As is well known, this procedure attenuates multiple reflections and other undesirable incoherent and coherent noise. A first approximation to the stacked section is the common-offset section calculated with the nearest receiver. This approach avoids the velocity analysis and stacking stages. A cheaper way is to compute the response of the model to a plane wave coming from the surface. The resulting section contains more diffractions and multiple events than the stacked section. Finally, a better approximation is obtained with the so-called exploding reflector technique which is free of multiples and diffractions, although this approach is less efficient in terms of memory storage and computer time. The plane wave and exploding reflector approaches are also compared in the elastic case where an appropriate equation based on constant P and S impedances has been obtained. As expected, both techniques show dissimilar results since the responses depend in this case on the nature (radiation pattern) of the source and the presence of mode conversion in the plane wave seismograms.

KEY WORDS: CMP section, plane wave response, exploding reflector, data processing.

INTRODUCTION

Forward modelling techniques have a variety of applications in geophysical prospecting. For instance, they are useful to demonstrate the consistency of interpretation of real seismic data, to provide synthetic seismograms for testing processing algorithms and acquisition parameters, and

0963-0651/94/$5.00

as a didactic tool to teach the geophysicist wave-propagation phenomena. An excellent example of the application of modelling to processing and interpretation is given by Kelly et al. (1982). In this work they assume a model containing a hydrocarbon reservoir, generate a set of common shots, produce the stacked section with several degrees of folding, and apply to this section a variety of processing algorithms. Moreover, they show how, with the use of snapshots, the events corresponding to the different material interfaces can be followed as they propagate through the model. Recently, Fagin (1992) published a series of case histories which illustrate how modelling can be used to better define complex structures. In particular, Morse, Purnell and Medwedeff compare synthetic data generated with the exploding reflector wave equation to the CMP stack of synthetic shot records.

In this paper we compare different techniques for computing a zero-offset seismic section. Two efficient ways, which avoid calculation of the common-shot synthetic records, are the plane-wave, and the exploding-reflector techniques. The first consists in sending a horizontal homogeneous plane wave down from the surface and recording the response of the model at the surface. In the exploding-reflector method (Baysal, Kosloff and Sherwood, 1984), each reflection point in the subsurface explodes at $t = 0$ with a magnitude proportional to the normal incidence reflection coefficient. The equation used in this case is a modification of the full wave equation where the impedance is constant over the whole model space. In this way, multiple reflections are avoided and the recorded events are primary energy. Moreover, the method generates normal-incidence reflections, i.e., those having identical downgoing and upgoing wave paths. The results from both methods are compared to the CMP stacked section and to common-offset sections obtained from the closest receivers. In the elastic case, we compare plane-wave and exploding-reflector seismograms due to vertical impulse sources.

THE WAVE EQUATION

Acoustic rheology

The constitutive equation representing a (2-D) acoustic medium is

$$-p = \varrho c^2 \epsilon \quad , \tag{1}$$

where $p(x,z,t)$ is the pressure field, $\epsilon(x,z,t)$ is the dilatation, $\varrho(x,z)$ is the density and $c(x,z)$ is the wave velocity. On the other hand, the equations of conservation of linear momentum (or Newton's equations) are

$$-(\partial p/\partial x) = \varrho(\partial^2 u_x/\partial t^2) + f_x \quad , \tag{2a}$$

and

$$-(\partial p/\partial z) = \varrho(\partial^2 u_z/\partial t^2) + f_z \quad , \tag{2b}$$

where (u_x,u_z) is the displacement vector, and (f_x,f_z) is the body-force vector. Dividing both sides of (2) by the density and taking the divergence yields

$$-(\partial/\partial x)\{(1/\varrho)(\partial p/\partial x)\} - (\partial/\partial z)\{(1/\varrho)(\partial p/\partial z)\} =$$

$$(\partial^2\epsilon/\partial t^2) + (\partial/\partial x)(f_x/\varrho) + (\partial/\partial z)(f_z/\varrho) \quad . \tag{3}$$

Replacing the stress-strain relation (1) into the r.h.s. of equation (3), the explicit form of the pressure-wave equation is

$$\varrho c^2[(\partial/\partial x)\{(1/\varrho)(\partial p/\partial x)\} + (\partial/\partial z)\{(1/\varrho)(\partial p/\partial z)\}] = (\partial^2 p/\partial t^2) + s \tag{4}$$

where

$$s = -\varrho c^2[(\partial/\partial x)(f_x/\varrho) + (\partial/\partial z)(f_z/\varrho)] \quad . \tag{5}$$

For constant density, equation (4) simplifies to

$$(\partial^2 p/\partial x^2) + (\partial^2 p/\partial z^2) = (1/c^2)(\partial^2 p/\partial t^2) + s \quad . \tag{6}$$

For a medium with homogeneous impedance the density can be written as

$$\varrho = K/c \quad , \tag{7}$$

where K is a constant. Substitution of (7) into (4) gives the non-reflecting wave equation

$$c(\partial/\partial x)\, c(\partial p/\partial x) + c(\partial/\partial z)\, c(\partial p/\partial z) = \partial^2 p/\partial t^2 + s \quad . \tag{8}$$

This equation has the properties that the normal-incidence reflection coefficient vanishes and that for homogeneous media it becomes the full acoustic wave equation (6) (Baysal et al., 1984).

Elastic rheology

In 2-D space, the elastic stress-strain relations read

$$\sigma_{xx} = \varrho\{c_P^2\epsilon - 2c_S^2(\partial u_z/\partial_z) \quad , \tag{9a}$$

$$\sigma_{zz} = \varrho\{c_P^2\epsilon - 2c_S^2(\partial u_x/\partial_x) \quad , \tag{9b}$$

$$\sigma_{xz} = \varrho c_S^2\{(\partial u_x/\partial_z)(\partial u_z/\partial_x) \quad , \tag{9c}$$

where c_P and c_S are the compressional and shear-wave velocities. In order to describe wave motion, relations (9a-c) are introduced into the force equilibrium equations

$$(\partial\sigma_{xx}/\partial x) + (\partial\sigma_{xz})/(\partial z) = \varrho(\partial^2 u_x/\partial t^2) + f_x \quad , \tag{10a}$$

$$(\partial\sigma_{xz}/\partial x) + (\partial\sigma_{zz})/(\partial z) = \varrho(\partial^2 u_z/\partial t^2) + f_z \quad . \tag{10b}$$

For homogeneous impedance regions, ϱc_P and ϱc_S are constants. In this case, following the same procedure to obtain (8), the non-reflecting elastic-wave equation is

$$c_P(\partial/\partial x)c_P\{(\partial u_x/\partial x) + (\partial u_z/\partial z)\} - 2c_S(\partial/\partial x)c_S(\partial u_z/\partial z)$$

$$+ c_S(\partial/\partial z)c_S\{(\partial u_x/\partial z) + (\partial u_z/\partial x)\} = \partial^2 u_x/\partial t^2 + s_x \quad , \tag{11a}$$

and

$$c_P(\partial/\partial z)c_P\{(\partial u_x/\partial x) + (\partial u_z/\partial z)\} - 2c_S(\partial/\partial z)c_S(\partial u_x/\partial x)$$

$$+ c_S(\partial/\partial x)c_S\{(\partial u_x/\partial z) + (\partial u_z/\partial x)\} = \partial^2 u_z/\partial t^2 + s_z \quad , \tag{11b}$$

where $s_x = f_x/\varrho$ and $s_z = f_z/\varrho$. Equations (11a-b) have also been obtained by Selvi (1991).

The time integration of equations (4) and (8) is carried out with a second-order (staggered) differencing technique. On the other hand, the elastic equations (10a-b) are solved with the rapid expansion method (REM)(Kosloff et al., 1989). The spatial derivatives are computed by using the Fourier method. The spectral coefficients of the wavefield are computed with the Fast Fourier Transform (FFT), based on a vectorized version of the mixed-radix FFT (Temperton, 1983). This differential operator is infinitely accurated up to the Nyquist wavenumber, which corresponds to a spatial wavelength of two grid points. This means that if our source is band-limited, the algorithm is free of numerical dispersion, provided that the grid spacing is chosen $D_Y \leq c_{min}/2f_{max}$, with f_{max} the cut-off frequency and c_{min} the minimum phase velocity in the mesh. In order to eliminate wraparound effects from the boundaries of the mesh, produced by the periodic properties of the Fourier method), the modelling includes an absorbing strip along these boundaries (Kosloff and Kosloff, 1986).

SIMULATIONS

The first geological model is illustrated in Fig. 1, where the compressional velocities are indicated in km/s (the density is constant). The

velocity anomaly at the center of the model (the velocity field is linearly interpolated from 3.5 to 2.8 m/s) is a challenge for most ray-tracing techniques: the anomaly produces an energy-focusing effect with the corresponding caustics. The number of grid points to obtain the common-shots records and the plane-wave response are $N_x = 800$ and $N_z = 180$, with a uniform grid spacing of DX = DZ = 15 m. These choices imply that the mesh propagates a wavelet with a maximum frequency of $f_{max} = c_{min}/2D_{max} = 66.7$ Hz, where c_{min} is the minimum phase velocity and $D_{max}$is the maximum grid spacing. The source is introduced as follows: numerically, a 1-D space delta is given by 1/DY (Y = X or Z). This comes from the fact that each spatial sample is represented by a sinc function with argument $\pi y/DY$. The integral of this function is precisely DY. Introduction of a discrete delta will alias the wavenumbers beyond the Nyquist (π/DY) to the lower wavenumbers. However, if the source time function h(t) is band-limited with cut-off frequency f_0, the wavenumbers greater than $k_0 = 2\pi f_0/c_{min}$ are automatically filtered. The following source function is used:

$$h(t) = e^{-2 f_0^2 (t-t_0)^2} \cos[2\pi f_0(t-t_0)] \quad , \tag{12}$$

where $f_0 = 60$ Hz and $t_0 = 50$ ms is a constant time delay introduced for causality considerations. The amplitude spectrum of h(t) is

$$\tilde{h}(\omega) = \pi(\pi/2)^{1/2}(1/\Omega_0)\exp(i\omega t_0)[\exp\{-(\pi^2/2)(1-\omega/\Omega_0)^2\}$$
$$+ \exp\{-(\pi^2/2)(1+\omega/\Omega_0)^2\}] \quad , \tag{13}$$

where $\Omega_0 = 2\pi f_0$. The amplitude spectrum of the source is represented in Fig.2, where it is clear that the dominant frequency is 30 Hz.

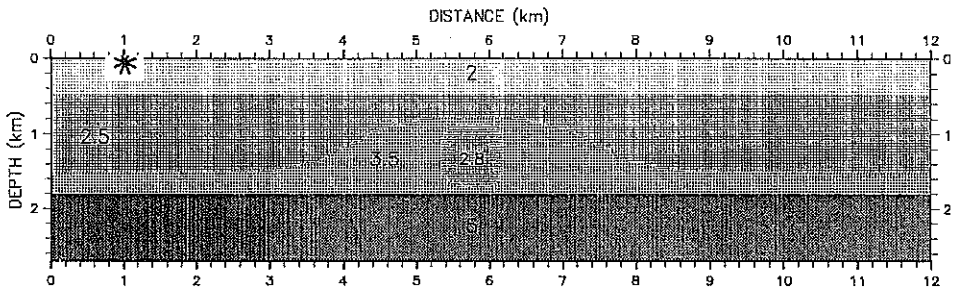

Fig. 1. Geological model containing an anticline-like structure and a velocity anomaly at the center. The numbers indicate the compressional wave velocity in km/s. In the anomaly, the velocity field is linearly interpolated from 3.5 to 2.8 m/s.

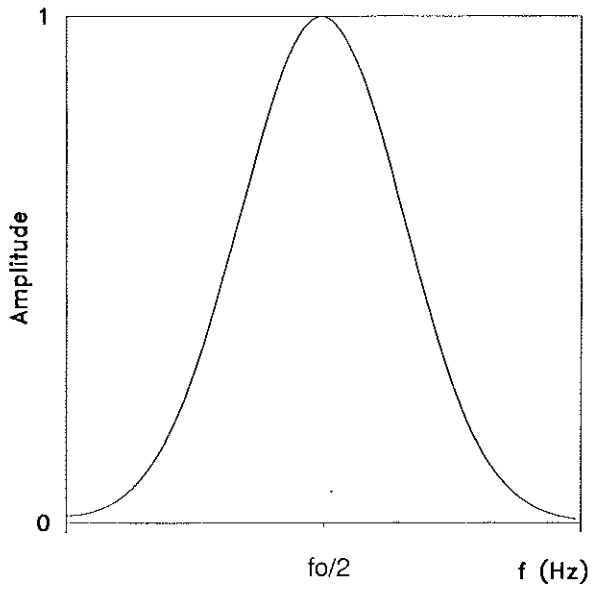

Fig. 2. Amplitude spectrum of the source. The dominant frequency is f_0 = 30 Hz.

The modelling program uses a mixed radix FFT routine with factors 2, 3, 4, 5 and 6 (Temperton, 1983). For first derivative calculations it is necessary to use odd-based FFT's. This is because even transforms have a Nyquist component which does not posses the Hermitian property of the derivative (e.g. that a derivative of an even function is odd, and viceversa). Therefore, grid numbers are composed with factors 3 and 5. The solution is propagated to 2 s with a time step dt = 1 ms. This value satisfies the stability condition of the integration scheme, by which $dt \leq D_{min}/\sqrt{2}\, c_{max}$ = 2 ms.

In order to simulate eight-fold CMP acquisition, 63 records were computed with the shot and 48 receivers moving from left to right in increments of 135 m per shot. The distance between adjacent receivers is 45 m, i.e., an array length of approximately 2 km. The position of the first shot is indicated in Fig. 1 by a star. Two common-offset sections, obtained from the nearest and farthest offsets, respectively, are illustrated in Fig. 3. The first one closely resembles the geological structure and is an approximation to the stacked section. In the second, the events are vertically compressed. Fig. 4 shows the stacked section.The high amplitude at the anticline is probably due to a constructive interference of the plane interface and anticline wavefields at long offsets (see Fig. 3).

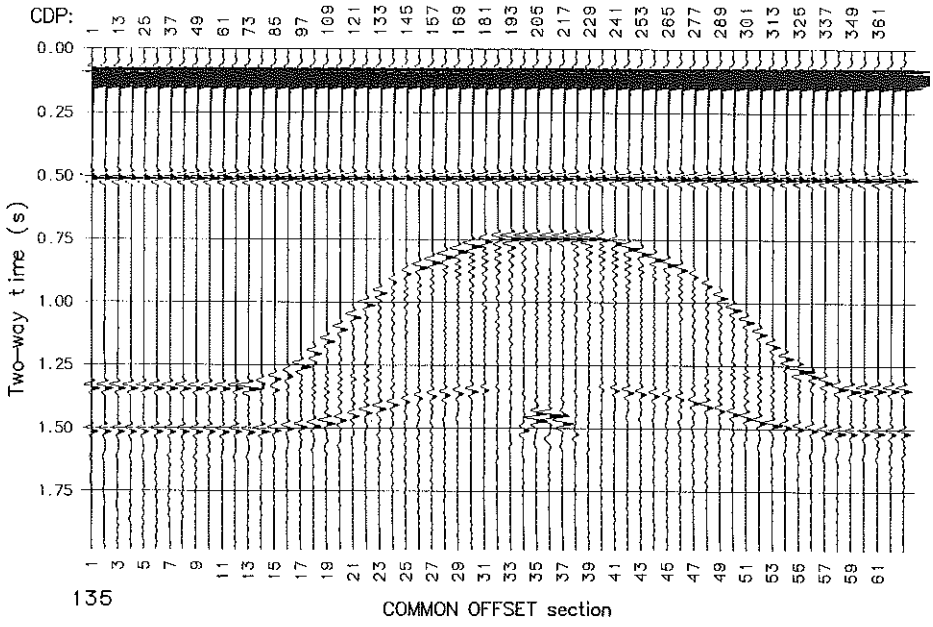

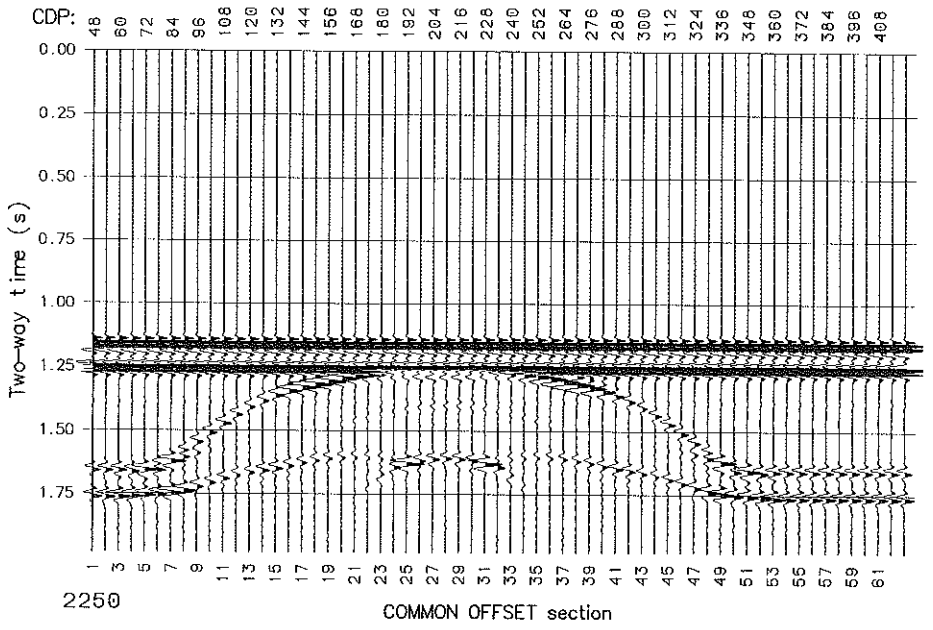

Fig. 3. Two common-offset seismograms corresponding to the nearest (top) and farthest (bottom) offsets, respectively.

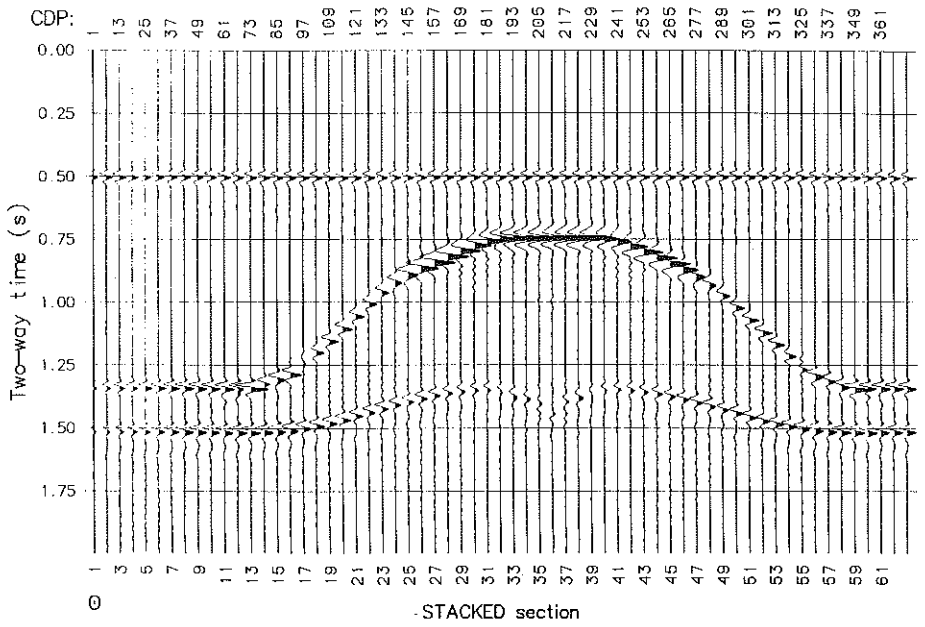

Fig. 4. Five-fold CMP section. 63 shots, 48 receivers, 2250 maximum offset. The high amplitude at the anticline is probably due to a constructive interference of the plane interface and anticline wavefields at far offsets (see Fig. 3).

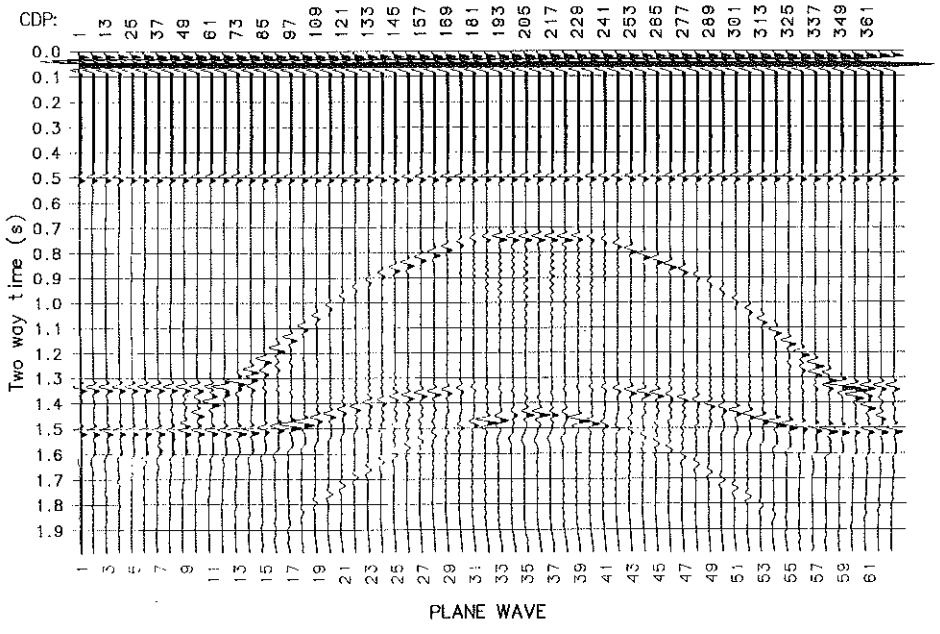

Fig. 5. Plane wave response. The seismogram contains noticeable diffractions compared to the exploding reflector seismogram represented in Fig. 7.

Fig. 5 displays the plane wave section. At the top of the seismogram the plane wave direct response can be appreciated. The section shows notable diffractions from the lower flanks of the anticline. Note that, as in the preceding cases, the response of the lower interface, at the center of the model, can be confused with the response of a syncline. This effect is caused by the presence of the velocity anomaly. In general, the plane wave response contains noticeable diffraction effects and weak multiple reflections. The presence of multiples makes this approach suitable for testing multiple-suppression techniques, as pointed out by Claerbout (1985, p. 358).

Fig. 6 shows the exploding reflector section, which is the solution of equation (11). Since the velocities are halved, in order to propagate the same pulse as in the preceding cases, we also halved the grid spacing, which implies doubling the number of grid points in each direction (actually, to the nearest odd number). Note that this makes the modelling more expensive than in the plane wave case. In addition, the calculation of the spatial derivatives in equation (11) is more time-consuming than in equation (9) (here, a second-order spatial derivative is computed by using only two Fourier transforms). As mentioned in the introduction, the strength of each reflector source is proportional to the reflection coefficient at the reflection point. This produces a realistic distribution

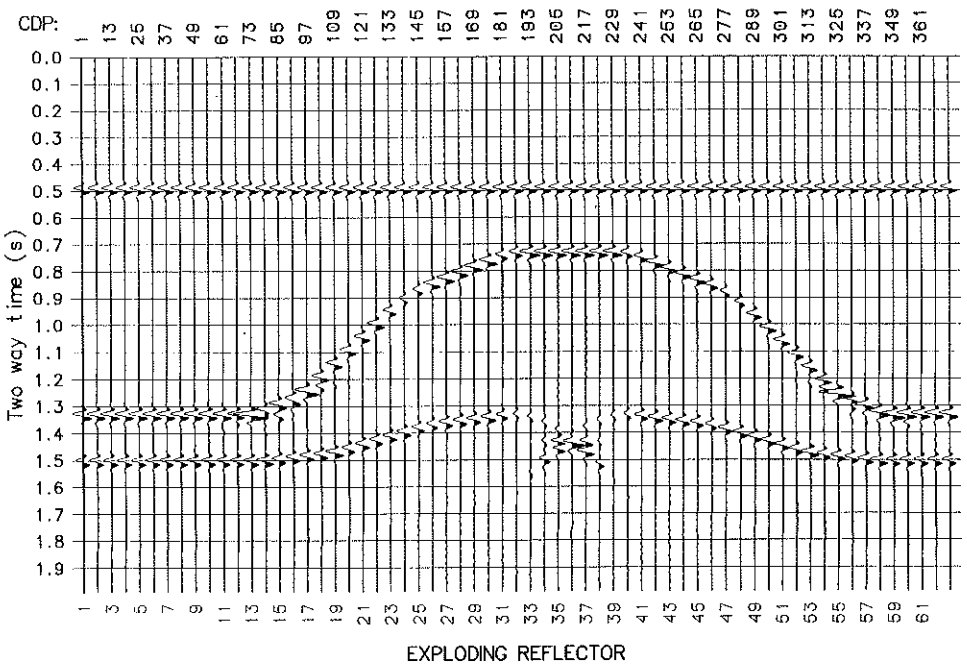

Fig. 6. Exploding reflector response. This seismogram resembles the stacked section more than the plane wave seismogram.

of energy along the reflector, for instance, bright spots due to impedance contrast should be reproduced. The exploding reflector section is clearly free of multiple reflections and diffractions are attenuated with respect to the plane wave response. Moreover, the response of the deeper interface below the velocity anomaly closely resembles that of the stacked section, despite the fact that the focussing effect of the anomaly may produce rays (in the stacked section) that are not predicted by the exploding reflector model (see Claerbout, 1985, p. 11). To better illustrate the focussing effect, we show in Figs. 7a and 7b a normal-incidence ray tracing and the corresponding arrival time diagram. As can be seen, the anomaly produces a syncline-type image of the lower interface.

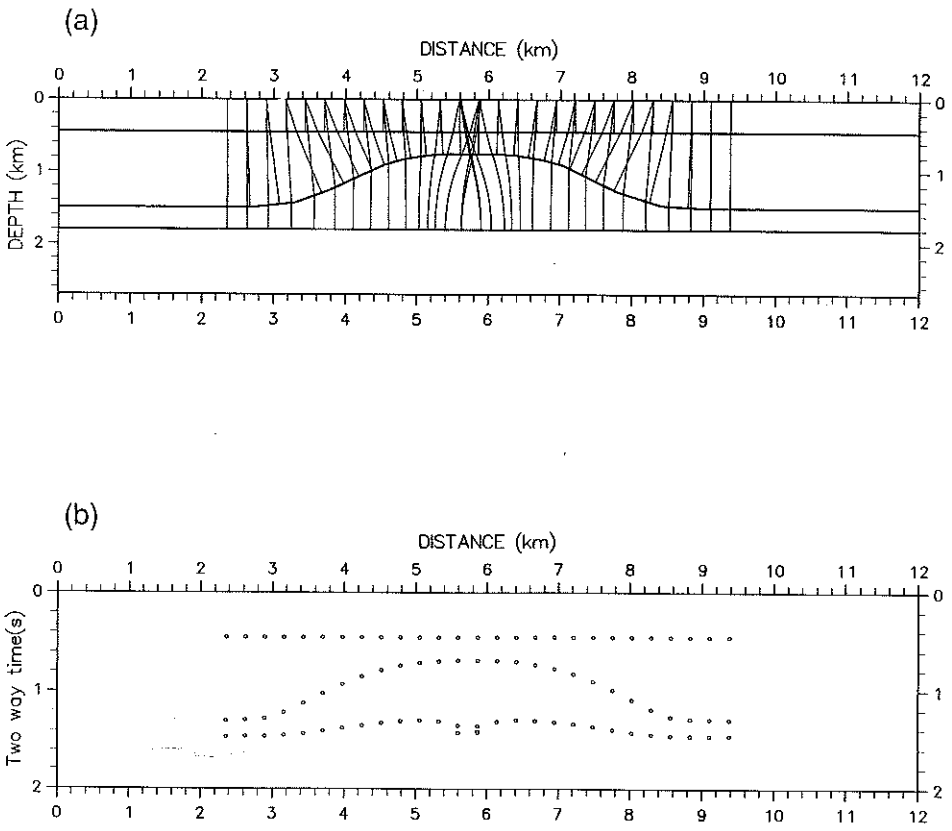

Fig. 7. Zero-offset ray tracing (a) and arrival time diagram (b) of the model represented in Fig. 1.

The second geological model is represented in Fig. 8, where the compressional and shear velocities are indicated. A zero-offset ray tracing, and its arrival time diagram, are shown in Figs. 9a and 9b, respectively. For a better visual comparison with the full wave seismograms, the rays are delayed by half the source duration. As is well known, since the focus of the syncline is below the receiver line, the time response does not resemble the original structure. The mesh to obtain the plane wave response has 125 × 125 points and 15 m grid spacing in both directions. The source has a maximum frequency of 50 Hz and consists of a vertical impulse at 300 m above the plane interface. The response is displayed in Figs. 10a and 10b, corresponding to pressure (divu) and shear (rotu) wave seismograms, respectively. The first seismogram contains the P response of both the plane interface and the syncline, since the energy from the source travels in the vertical direction. As expected, the plane interface does not reflect shear waves, unlike the syncline whose response arise from mode conversion (PS) at non-normal incidence angles, as can be appreciated in Fig. 9.

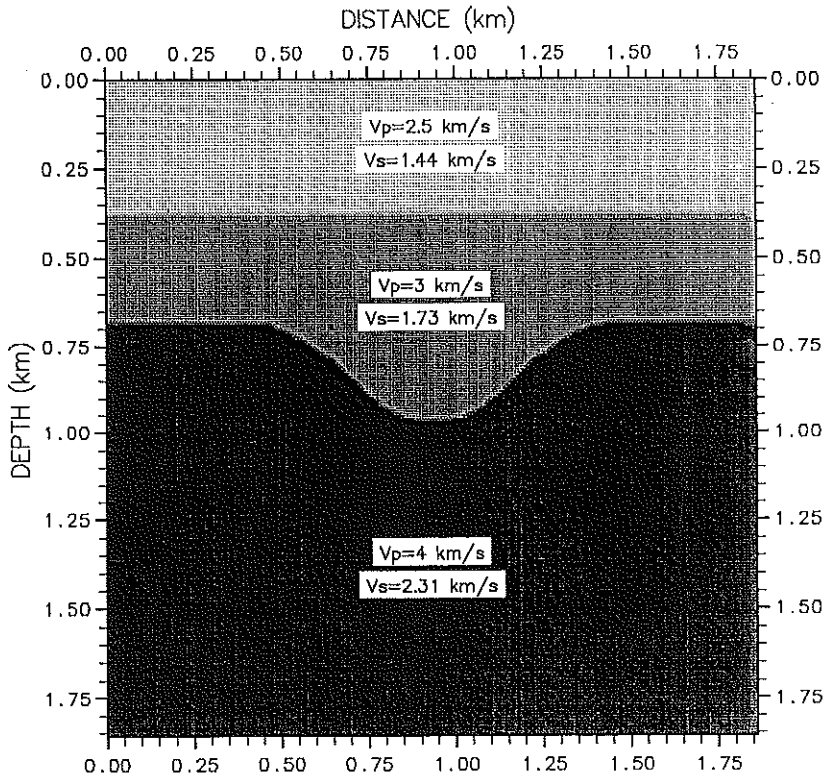

Fig. 8. Geological model consisting of a layer overlying a synclinal structure. The compressional and shear wave velocities are indicated in the figure. The density is constant.

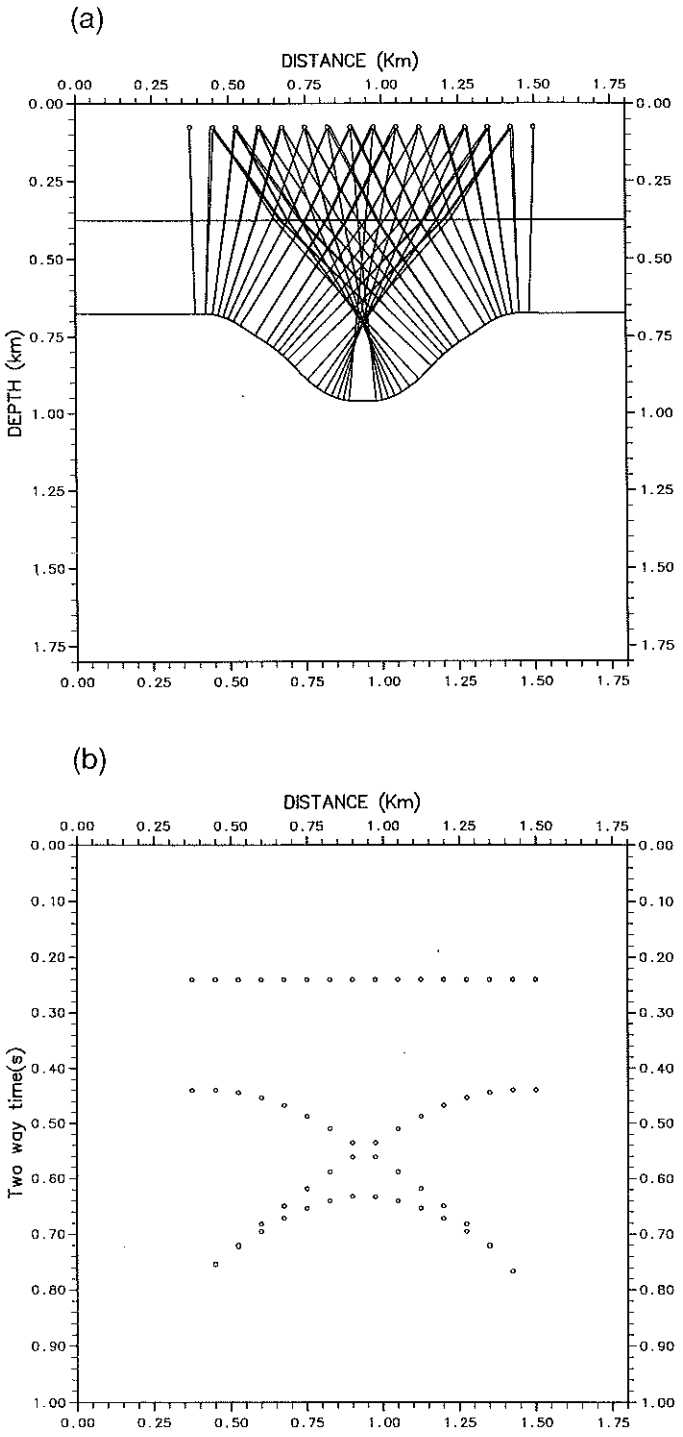

Fig. 9. Zero-offset ray tracing (a) and arrival time diagram (b) of the model represented in Fig. 8.

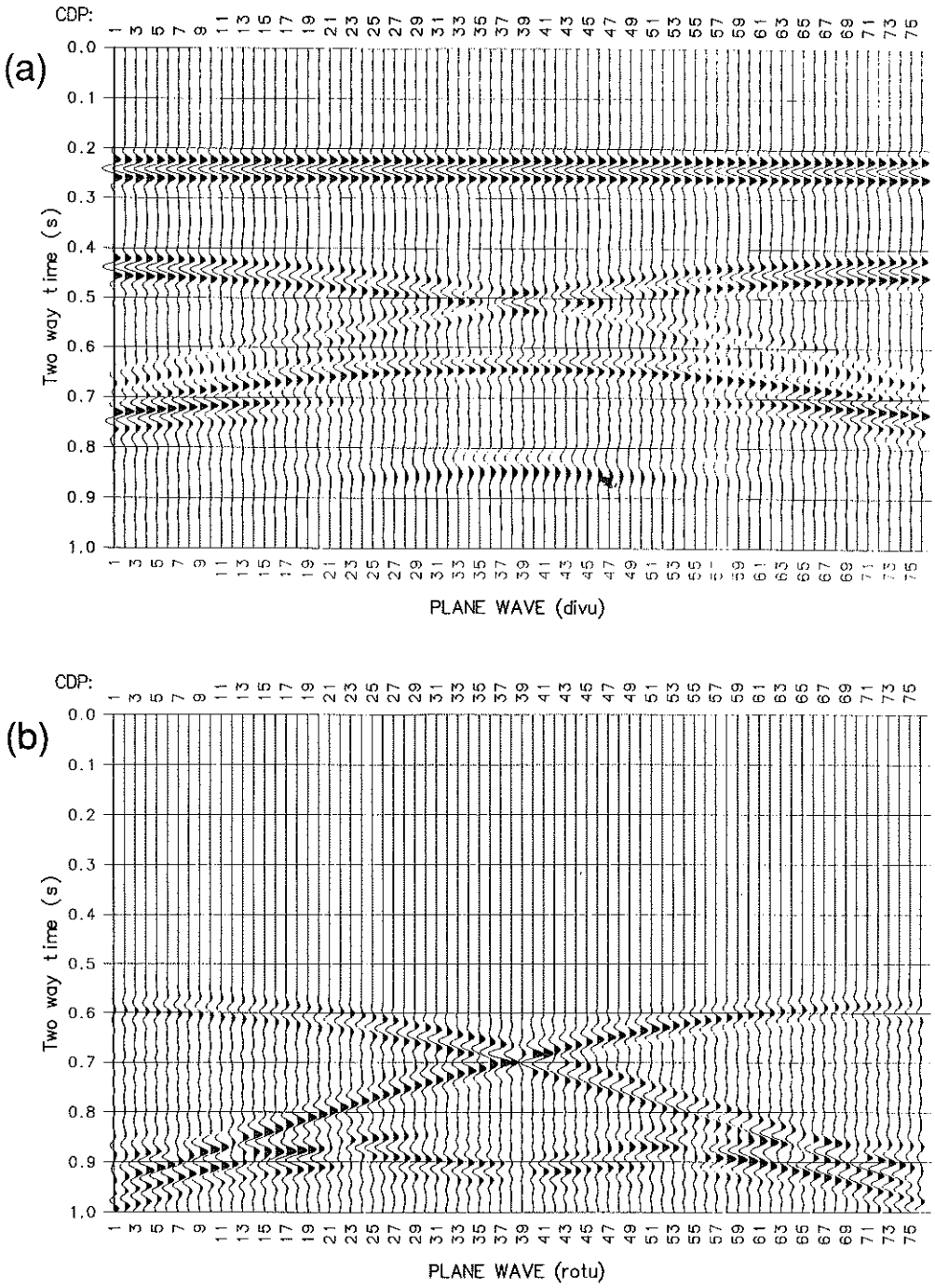

Fig. 10. (a) Compressional (divu) and (b) shear (rotu) wave seismograms of the syncline model due to a vertical plane wave source. The response of the anticline in (b) is due to mode conversion at non-normal incident angles.

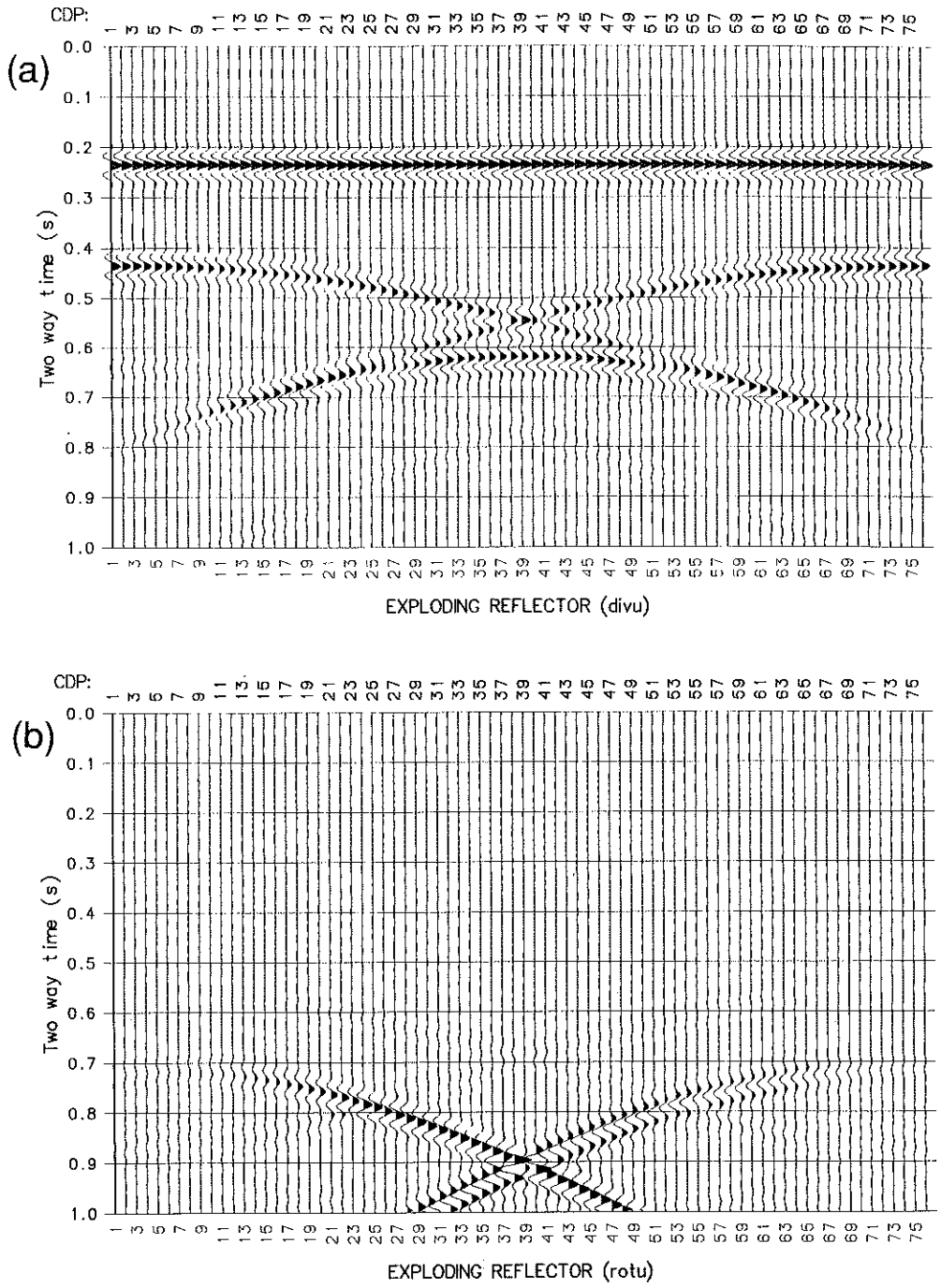

Fig. 11. (a) Compressional (divu) and (b) shear (rotu) wave seismograms of the syncline model in the elastic exploding reflector case. Compared to Fig. 10, the response of the syncline shows notable differences.

On the other hand, the exploding reflector mesh has 243 × 243 grid points and 7.5 m grid spacing. The source is again a vertical impulse at each interface grid point. The response is shown in Figs. 11a and 11b which correspond to the pressure and shear seismograms, respectively. As can be seen, the response of the plane interface is compressional only since, as before, the source does not radiate shear waves in the vertical direction. However, the syncline produces shear waves out of the vertical direction, and its response can be clearly seen in Fig. 11b. Comparing Figs. 10a and 11a, we note that the syncline responses are different, mainly due to the presence of diffractions in the plane wave case. The arrival times of the bow-tie reflections in Figs. 10a and 11a differ by approximately 40 ms. From the arrival time diagram displayed in Fig. 9a, it can be seen that the exploding reflector seismogram approaches the zero-offset ray tracing plot better than the plane wave response. Another difference is in the phase of the events, due to the fact that in the exploding reflector model there are no phase shifts since there are no reflections.

CONCLUSIONS

Wave equation synthetics are useful in recognizing patterns associated with different types of structures, and predicting some of the drawbacks when interpreting migrated and unmigrated sections of a given complex structure. As shown in this work, the presence of a velocity anomaly over a flat interface may produce some ambiguities in the final interpretation. This may be important when testing migration algorithms which perform the time-to-depth conversion of a seismic section. We compare two simulations of a zero-offset section which avoid calculation of the common-shot records. The response of the model to a horizontal plane wave contains noticeable diffractions and multiple reflections, and could be useful to test the robustness of the migration algorithm in the presence of these coherent noises. On the other hand, the exploding reflector is free of multiples, and diffraction noise is weaker than in the plane wave case. Moreover, the resulting section closely resembles the CMP section, in particular in the region where the anomaly affects the response of the deeper interface. The approach is useful in modelling or reverse-time migration when it is necessary to avoid interlayer reverberations. In the elastic case, we compare plane wave and exploding reflector seismograms of a syncline below a plane interface. The modelling gives here the possibility of computing four kinds of seismogram. These are the two displacement components, and the purely P and purely S responses through the calculation of the divergence and curl of the displacement vector, respectively. Mode conversion and diffractions in the plane wave case accentuate the differences between the two approaches. Application of elastic migration algorithms could produce very dissimilar results.

ACKNOWLEDGEMENTS

This work was supported in part by the Commission of the European Communities under the GEOSCIENCE project.

REFERENCES

Baysal, E., Kosloff, D.D. and Sherwood, J.W.C., 1984. A two-way nonreflecting wave equation. Geophysics, 49: 132-141.

Claerbout, J.F., 1985. Imaging the Earth's Interior. Blackwell Scientific Publications, Oxford.

Fagin, S. W., 1992. Seismic Modelling of Geological Structures; Applications to Exploration Problems. SEG Publications, Tulsa.

Kelly, K.R., Alford, R.M. and Whitmore, N.D., 1982. Modeling - the forward method. In: Jain, K.C. and deFiguereido, R.J.P. (Eds.), Concepts and Techniques in Oil and Gas Exploration, SEG Publications, Tulsa, OK.

Kosloff, R. and Kosloff, D., 1986. Absorbing boundaries for wave propagation problems. J. Comp. Phys., 63: 363-376.

Kosloff, D., Queiroz Filho, A., Tessmer, E. and Behle, A., 1989. Numerical solution of the acoustic and elastic wave equations by a new rapid expansion method. Geophys. Prosp., 37: 383-394.

Selvi, O., 1991. The modified elastic wave equation applied to modelling and migration. EAEG, 53rd Mtg., Florence, Italy, Expanded Abstr.: 598-599.

Temperton, C., 1983. Fast mixed radix real Fourier transforms. J. Comp. Phys., 52: 340-350.